Thermal spin transport properties of magnetic C_{28} monomolecular devices

LI QIANG[a,b,*], YANG YONG-MING[a,b], REN DA-HUA[c], MENG GAO-XIANG[a,b]
[a]*School of Advanced Materials and Mechatronic Engineering, Hubei Minzu University, Enshi 445000, China*
[b]*Institute of University-industry Cooperation for Advanced Material Forming and Equipment, Hubei Minzu University, Enshi 445000, China*
[c]*School of Information Engineering, Hubei Minzu University, Enshi 445000, China*

In this paper, we conduct a theoretical investigation on the thermal spin transport properties of three devices based on magnetic C_{28} monomolecular, using the non-equilibrium Green's function combined with density functional theory. By applying a temperature field, we observe that these devices lead to a spin-dependent Seebeck effect; some devices also embody spin-dependent Seebeck diode effect and negative differential resistance effect. The physical mechanism was explained using the Fermi-Dirac distribution and spin transmission spectrum. These interesting effects suggest that these three devices can be used as new spin nanodevices.

(Received April 13, 2020; accepted June 11, 2021)

Keywords: Monomolecular device, Spin-dependent Seebeck effect, Spin-dependent Seebeck diode effect, Negative differential resistance effect

1. Introduction

Molecular spintronic devices, in which molecules are used as spin transport channels, have been attracting the attention of researchers. Spin caloritronics, the combination of spintronics with thermoelectrics, examines the interaction between heat flow, spin current, and charge current in materials [1-8]. Spin caloritronics has attracted increasing attention since it holds promise for the next generation of electronic devices, enhanced functionality and improved performances, in high-density information storage and quantum computing [9-11]. Recently, many researchers have mainly focused on fullerenes and their derivatives, C_{60}, C_{20}, C_{28}, and so on [12-18]. The C_{28} molecule consists of a tetrahedral cage with four unpaired electrons in a $^5A_2$ open-shell ground state of T_d symmetry [19-22]. Experimental and theoretical investigations have mainly focused on the stability, electronic structure, and superconductivity of C_{28} and its derivatives. Andrey et al. reported the structure, electronic properties, and intercalates of C_{28} fullerites, and it showed that their properties could be tuned by intercalation with Zn, Ti, and K [19]. Xu et al. reported the transport spin polarization of C_{28} molecular junctions, and it showed that the transport spin polarization could be tuned effectively by the gate voltage[23]. However, to date, the research on small fullerene molecules has been limited. To the best of our knowledge, the thermal spin transport properties of C_{28} molecular junctions are yet to be reported.

In this paper, magnetic C_{28} monomolecular devices are fabricated by attaching a C_{28} molecule to the Au(111) surface with sulfur atoms. We studied the thermal spin transport properties of these magnetic C_{28} monomolecular devices by temperature field. The results show that the spin-dependent Seebeck effect (SDSE), spin-dependent Seebeck diode effect (SDSD), and negative differential resistance effect (NDR) exist in the magnetic C_{28} monomolecular devices.

2. Model and theoretical method

The magnetic C_{28} monomolecular devices were fabricated by attaching a C_{28} molecule to an Au(111) surface with sulfur atoms. The C_{28} molecule with T_d symmetry has four hexagons and twelve pentagons. There are three types of inequivalent carbon atoms, which were labeled as C_1, C_2, and C_3, respectively, as shown in Fig. 1(a). The calculated local atomic magnetic moment of C_1, C_2, and C_3 atoms is 0.26, -0.07, and 0.45 μ_B, respectively. The molecular magnetic moment of C_{28} is predicted to be 4 μ_B [23-25]. Fig. 1(b)-(d) depicts these three types of carbon atoms of the C_{28} molecule were attached to the Au(111) surface with sulfur atoms, and the devices were each denoted as DEV_1, DEV_2, and DEV_3, respectively.

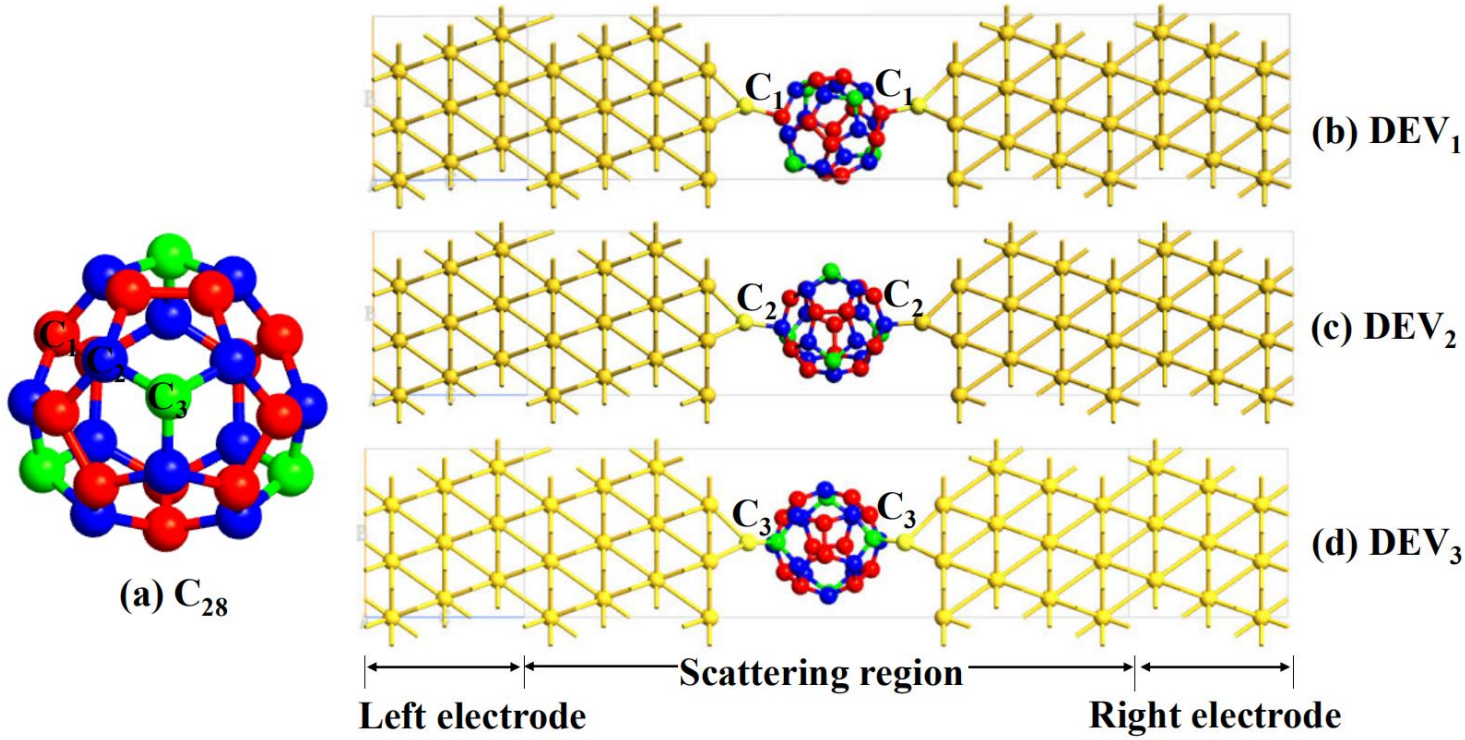

Fig. 1. (a) The geometry structure of the C_{28} molecule with T_d symmetry top view, the red, blue and green balls stand for three types of inequivalent carbon atoms, named as C_1, C_2 and C_3, respectively. The model of the magnetic C_{28} monomolecular device (b) DEV_1, (c) DEV_2 and (d) DEV_3 (color online)

In this paper, the calculations performed using the non-equilibrium Green's function (NEGF) combined with the density functional theory (DFT), which is contained in the Atomistix ToolKit (ATK) package [26-28]. The core electrons were described by using norm-correlation pseudo-potentials, and the Local-density approximation (LDA) was used in the exchange-correlation potential [29,30]. A single-polarized basis set was used with a cutoff energy of 150 Ha and a Monkhorst-Pack k-point grid of 1×1×100. The convergence parameters for optimization were 1×10^{-5} eV for total energy tolerance and 0.005 eV/Å for maximum force tolerance. The spin-dependent current is given by[31]

$$I^{\uparrow(\downarrow)} = \frac{e}{h}\int_{-\infty}^{\infty}\{T^{\uparrow(\downarrow)}(E)[f_L(E,T_L) - f_R(E,T_R)]\}dE \tag{1}$$

where $I^{\uparrow(\downarrow)}$ is denote the spin-up (spin-down) current, $f_{L,R}(E,T_{L,R})$is the equilibrium Fermi distribution for the left (right) electrode. $T^{\uparrow(\downarrow)}(E)$ is the spin-resolved transmission, defined as

$$T^{\uparrow(\downarrow)}(E) = Tr\left[\Gamma_L G^R \Gamma_R G^A\right]^{\uparrow(\downarrow)} \tag{2}$$

where $G^{R(A)}$ is the retarded (advanced) Green's function of the central region and $\Gamma_{L(R)}$ is the coupling matrix of the left (right) electrode.

3. Results and discussion

To study the thermal spin transport properties of the magnetic C_{28} monomolecular devices, we applied a temperature field to the left and right electrodes of the device without an external bias voltage. The temperatures of the left and right electrodes were denoted by T_L and T_R, respectively. The T_L was always higher than T_R, and the temperature difference between the left and right electrodes was defined as $\Delta T=T_L-T_R$. The thermal spin-dependent currents were denoted by spin-up currents ($I^{\uparrow}$) and spin-down currents ($I^{\downarrow}$), the total spin current was denoted by I_s ($I_s = I^{\uparrow} - I^{\downarrow}$), and the net charge current was denoted by I_c ($I_c = I^{\uparrow} + I^{\downarrow}$).

Fig. 2 shows the relationships between the currents ($I^{\uparrow}$, $I^{\downarrow}$, I_s, and I_c) and T_L for DEV_1, DEV_2, and DEV_3, where ΔT

was set to 20, 40, and 60 K, respectively. Fig. 2(a) shows the spin-dependent currents as a function of T_L for DEV_1. We found a negative $I^{\uparrow}$ appeared and a positive $I^{\downarrow}$ was present at the same time, and the magnitude of $I^{\downarrow}$ was almost the same as $I^{\uparrow}$. It showed that an SDSE existed in DEV_1 [32-34]. Moreover, $I^{\uparrow}$ and $I^{\downarrow}$ increased with T_L, then decreased with increasing T_L after reaching a certain temperature, indicates a spin-dependent negative differential resistance effect appeared. I_c and I_s followed similar trends, as shown in Fig. 2(b)–2(c), which means a spin-dependent negative differential resistance effect (NDR) appeared [32-36]. At the same time, $I_c << I_s$, it means spin current plays a significant role.

Fig. 2(d) shows the thermal spin-dependent currents ($I^{\uparrow}$ and $I^{\downarrow}$), I_s and I_c, as a function of T_L for DEV_2. These results showed that the device has a threshold temperature T_{th}, no spin-dependent current existed when $T_L < T_{th}$. When $T_L > T_{th}$, a positive $I^{\uparrow}$ and a negative $I^{\downarrow}$ appeared, indicates an SDSE occurred. However, the I_c increased with T_L, then decreased with increasing T_L after reaching a peak at approximately T_L = 200 K, which shows an NDR appeared. Moreover, $I^{\uparrow}$ was slightly bigger than $I^{\downarrow}$. Due to $I^{\uparrow}$ and $I^{\downarrow}$ flowing in opposite directions, and SDSE is generated by the spin-dependent currents induced by a temperature gradient. These results showed that I_c increased with the competition between $I^{\uparrow}$ and $I^{\downarrow}$, as shown in Fig. 2(e), I_s increased sharply from zero to approximately T_L = 200 K, which embodied an SDSD, as shown in Fig 2(f).

Fig. 2(g) shows the thermal spin-dependent currents, I_s and I_c, as a function of T_L for DEV_3. When $T_L < T_{th}$, there is not spin-dependent current, and when $T_L > T_{th}$, a negative $I^{\uparrow}$ and a positive $I^{\downarrow}$ appeared simultaneously. The thermal spin-dependent currents increased with T_L. Moreover, $I^{\downarrow}$ was a litter bit bigger than $I^{\uparrow}$. SDSE and NDR are generated by the spin-dependent currents. These results indicated that I_c increased with the competition between $I^{\uparrow}$ and $I^{\downarrow}$, as shown in Fig. 2(h), and I_s increased sharply from zero when T_L exceeded T_{th}, which embodied an SDSD, as shown in Fig. 2(i).

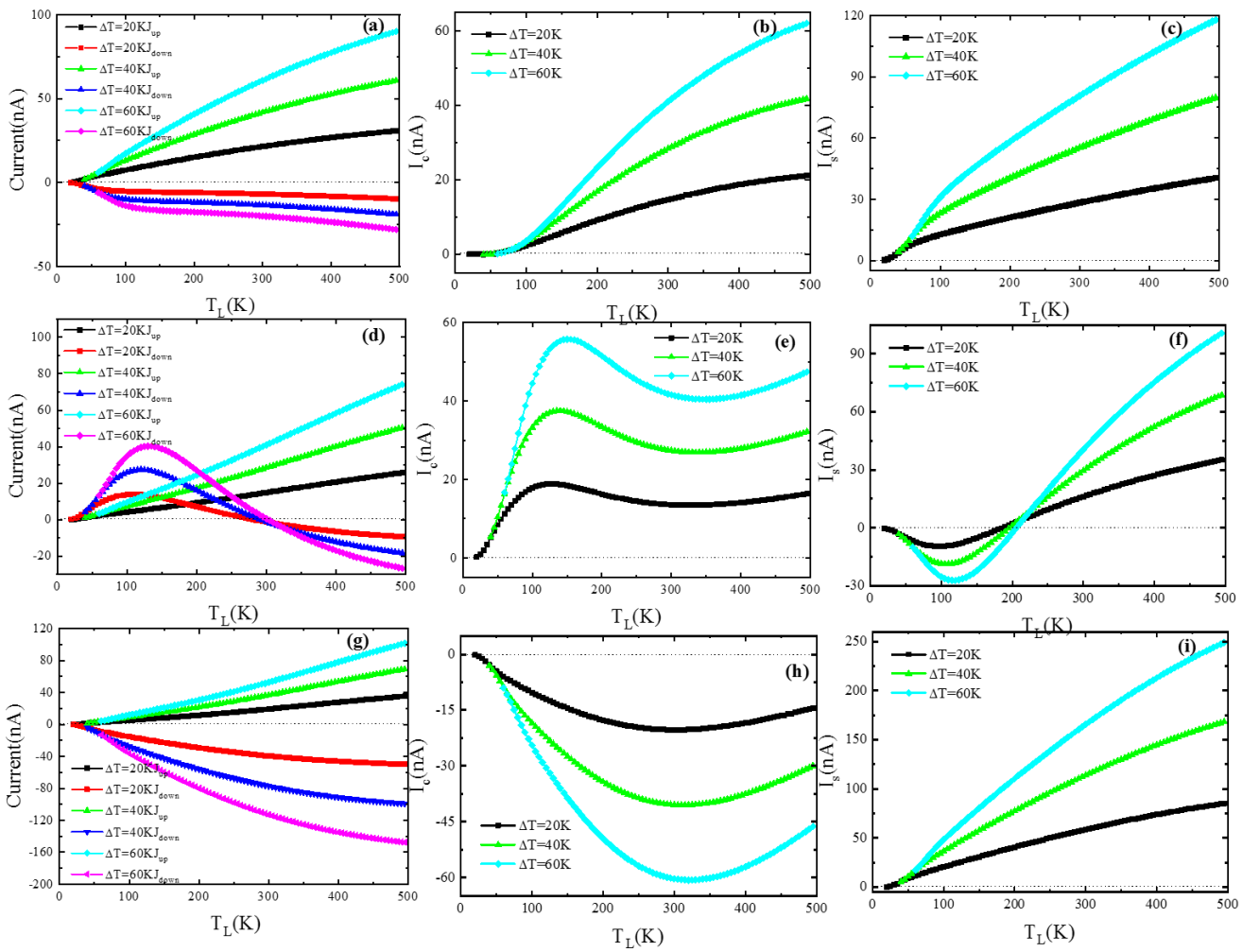

Fig. 2. The relationships between the thermal spin-depend currents, the total spin currents, the net charge currents and T_L of (a)-(c) DEV_1, (d)-(f) DEV_2, and (g)-(i) DEV_3 (color online)

To explain the mechanism of these interesting phenomena, we examined the transport spectra of these three devices, as shown in Fig. 3. When $T_L \neq T_R$, the distributions of the carriers in the left and right electrodes differed, as per the Fermi-Dirac distribution. The number of electrons above the Fermi level and holes below the Fermi level increased with ΔT. Because $T_L > T_R$, both electrons and holes moved from the left electrode to the right electrode, which formed a negative electron current I_e and a positive hole current I_h. The spin-dependent current is determined by the transmission coefficient of the system and the difference of the Fermi-Dirac distributions between the left and right electrodes. When the transmission spectrum was symmetric, I_e and I_h canceled each other, which resulted in $I_c = 0$. In this case, the transmission spectra were asymmetric about the Fermi level. For DEV_1, DEV_2, and DEV_3, the main transmission peaks of the spin-up channel were below the Fermi level, and the main transmission peaks of the spin-down channel were above the Fermi level, as shown in Fig. 3. Thus, the holes could move from the left electrode to the right electrode, which formed a positive $I^{\uparrow}$. Additionally, the electrons could move from the left electrode to the right electrode, which formed a negative $I^{\downarrow}$. There were many transmission peaks of the spin-up and spin-down channels above the Fermi level, so electrons moved from the left electrode to the right electrode. A peak of the negative thermal spin-down currents existed in DEV_1, as shown in Fig. 3(a). Similarly, the three main transmission peaks of the spin-down channel were above the Fermi level. Meanwhile, the two main transmission peaks of the spin-down channel were near the Fermi level. Some holes and electrons were near the Fermi level, so the holes and electrons moved from the left electrode to the right electrode, which formed a positive $I^{\uparrow}$ and negative $I^{\downarrow}$, respectively. However, the transmission peak below the Fermi level was larger than above the Fermi level. As a result, the peak of the positive thermal $I^{\downarrow}$ existed in DEV_2, as shown in Fig. 3(b). Similarly, a main transmission peak of the spin-down channel existed above and below the Fermi level, owing to the positive thermal spin-down currents and negative thermal spin-up currents in DEV_3, as shown in Fig. 3(c). The peak of the spin-up channels extended further below the Fermi surface, and the spin-down channels extended above the Fermi surface, but the magnitude of spin-up and spin-down channels are different, which resulted in a competition between $I^{\uparrow}$ and $I^{\downarrow}$, with the flows in opposite directions. The result was a single-spin differential resistance effect existed in DEV_2 and DEV_3, and an SDSE existed in the DEV_1, DEV_2, and DEV_3.

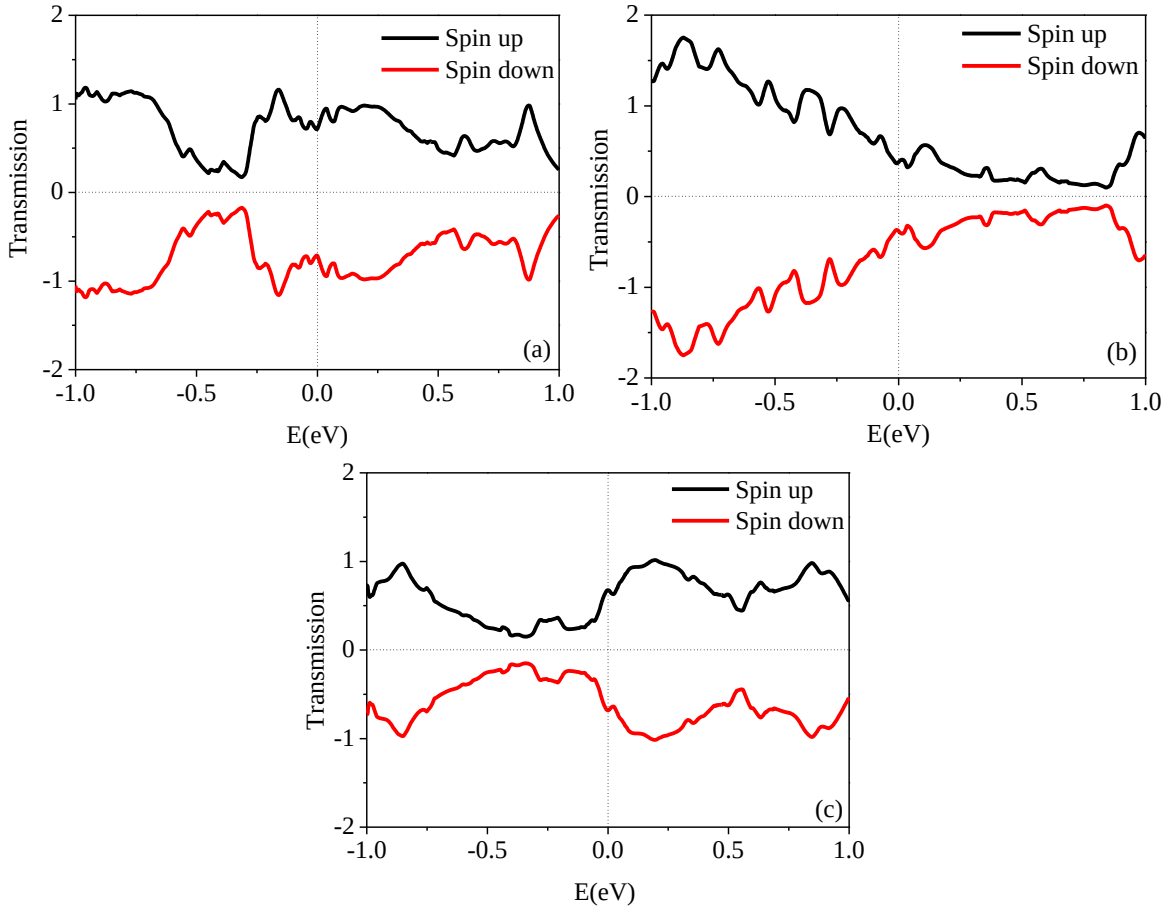

Fig. 3. Transmission spectra of (a) DEV_1, (b) DEV_2, and (c) DEV_3 (color online)

We examined the transmission pathway and electrostatic difference potential of these three devices, as shown in Fig. 4. The magnitude of the electrostatic difference potential is illustrated by the color, where a darker color corresponds to a larger magnitude. The transmission pathway is illustrated by the volume of the arrow, and the color represents the direction. The transmission pathways showed that the spin electrons could easily pass to these three devices.

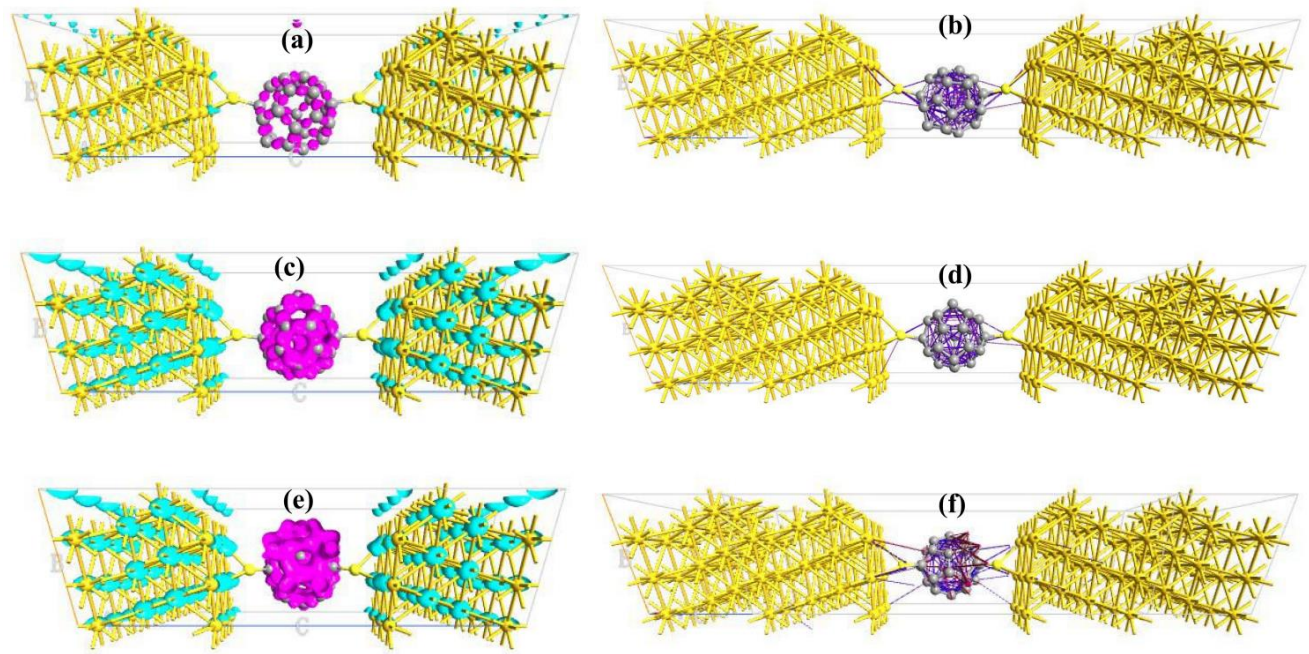

Fig. 4. Transmission pathway and electrostatic difference potential of (a) and (d) for the DEV_1, (b) and (e) for the DEV_2, (c) and (f) for the DEV_3, respectively (color online)

4. Conclusion

In this paper, we studied the thermal spin transport properties of magnetic C_{28} monomolecular devices by temperature field. The relationships between the thermal spin-depend currents, the total spin currents, the net charge currents and T_L of all three devices are obtained. The spin-dependent Seebeck effect appears in all three devices. Some devices also embody a spin-dependent Seebeck diode effect and a negative differential resistance effect. The physical mechanism was explained using the Fermi-Dirac distribution and spin transmission spectrum. We also examined the transmission pathway and electrostatic difference potential of these three devices. In summary, the results suggest that these three devices can be used as new spin nanodevices.

Acknowledgments

This work was supported by the Educational Commission of Hubei Province of China (Grant No.T201914), the Doctoral Research Foundation of Hubei Minzu University Project (Grant No. RZ1900003082).

References

[1] H. H. Fu, G. F. Du, D. D. Wu, Q. B. Liu, R. Q. Wu, Physical Review B **100**(8), 085407 (2019).
[2] X. Y. Tan, D. D. Wu, Q. B. Liu, H. H. Fu, R. Q. Wu, Journal of Physics: Condensed Matter **30**(35), 355303 (2018).
[3] X. Y. Tan, L. N. Zhang, L. L. Liu, Chemical Physics Letters **748**, 137386 (2020).
[4] J. Y. Xiao, X. Y. Tan, B. B. Yang, D. H. Ren, A. Y. Zuo, H. H. Fu, Acta Physica Sinica **68**(5), 057301 (2019).
[5] J. Yan, S. Wang, K. Xia and Y. Ke, Physical Review B **95**(12), 125428 (2017).
[6] N. Tombros, C. Jozsa, M. Popinciuc, H. T. Jonkman, B. J. van Wees, Nature **448**(7153), 571 (2007).

[7] K. Uchida, S. Takahashi, K. Harii, J. Ieda, W. Koshibae, K. Ando, S. Maekawa, E. Saitoh, Nature **455**, 778 (2008).
[8] G. E. Bauer, E. Saitoh, B. J. van Wees, Nature Materials **150**(11), 391 (2012).
[9] Z. H. Xiong, D. Wu, Z. Valy Vardeny, J. Shi, Nature **427**, 821 (2004).
[10] S. A. Wolf, D. D. Awschalom, R. A. Buhrman, J. M. Daughton, S. von Molnár, M. L. Roukes, A. Y. Chtchelkanova, D. M. Treger, Science **294**(5546), 1488 (2001).
[11] A. R. Rocha, V. M. García-suárez, S. W. Bailey, C. J. Lambert, J. Ferrer, S. Sanvito, Nature Materials **4**, 335 (2005).
[12] F. N. Ajeel, M. H. Mohammed, A. M. Khudhair, Russian Journal of Physical Chemistry B **11**(5), 850 (2017).
[13] S. Caliskan, Physica E: Low-dimensional Systems and Nanostructures **99**, 43 (2018).
[14] H. He, R. Pandey and S. P. Karna, Chemical Physics Letters **439**(1), 110 (2007).
[15] N. Sergueev, A. A. Demkov, H. Guo, Physical Review B **75**(23), 233418 (2007).
[16] L. H. Wang, Y. Guo, C. F. Tian, X. P. Song, B. J. Ding, Journal of Applied Physics **107**(10), 103702 (2010).
[17] X. Zheng, W. Lu, T. A. Abtew, V. Meunier, J. Bernholc, ACS Nano **4**(12), 7205 (2010).
[18] K. P. Katin, M. M. Maslov, Physica E: Low-dimensional Systems and Nanostructures **96**, 6 (2018).
[19] A. Enyashin, S. Gemming, T. Heine, G. Seifert, L. Zhechkov, Physical Chemistry Chemical Physics **8**(28), 3320 (2006).
[20] X. Lu, Z. Chen, Chemical Reviews **105**(10), 3643 (2005).
[21] N. A. Romero, J. Kim, R. M. Martin, Physical Review B **76**(20), 205405 (2007).
[22] P. R. C. Kent, M. D. Towler, R. J. Needs, G. Rajagopal, Physical Review B **62**(23), 15394 (2000).
[23] K. Xu, J. Huang, Z. Guan, Q. Li, J. Yang, Chemical Physics Letters **535**, 111 (2012).
[24] T. Guo, R. E. Smalley, G. E. Scuseria, The Journal of Chemical Physics **99**(1), 352 (1993).
[25] H. W. Kroto, D. R. M. Walton, Chemical Physics Letters **214**(3), 353 (1993).
[26] S. Smidstrup, D. Stradi, J. Wellendorff, P. A. Khomyakov, U. G. Vej-Hansen, M. E. Lee, T. Ghosh, E. Jónsson, H. Jónsson and K. Stokbro, Physical Review B **96**(19), 195309 (2017).
[27] S. Smidstrup, T. Markussen, P. Vancraeyveld, J. Wellendorff, J. Schneider, T. Gunst, B. Verstichel, D. Stradi, P. A. Khomyakov, U. G. Vej-Hansen, M.-E. Lee, S. T. Chill, F. Rasmussen, G. Penazzi, F. Corsetti, A. Ojanperä, K. Jensen, M. L. N. Palsgaard, U. Martinez, A. Blom, M. Brandbyge, K. Stokbro, Journal of Physics: Condensed Matter **32**(1), 015901 (2019)
[28] QuantumATK, version P-2019.03. https://www.synopsys.com/silicon/quantumatk.html.
[29] J. P. Perdew, A. Zunger, Physical Review B **23**(10), 5048 (1981).
[30] S. H. Vosko, L. Wilk, M. Nusair, Canadian Journal of Physics **58**(8), 1200 (1980).
[31] Y. Imry, R. Landauer, Reviews of Modern Physics **71**(2), S306 (1999).
[32] D. D. Wu, G. F. Du, H. H. Fu, Journal of Materials Chemistry C **8**(13), 4486 (2020).
[33] D. D. Wu, H. H. Fu, Q. B. Liu, R. Q. Wu, Journal of Materials Chemistry C **6**(39), 10603 (2018).
[34] D. D. Wu, H. H. Fu, Q. B. Liu, G. F. Du, R. Q. Wu, Physical Review B **98**(11), 115422 (2018).
[35] D. D. Wu, Q. B. Liu, H. H. Fu, R. Q. Wu, Nanoscale **9**(46), 18334 (2017).
[36] Z. Q. Zhang, Y. R. Yang, H. H. Fu, R. Q. Wu, Nanotechnology **27**(50), 505201 (2016).

*Corresponding author: 2012002@hbmzu.edu.cn